

Stair Climbing Stabilization of the HRP-4 Humanoid Robot using Whole-body Admittance Control

Stéphane Caron, Abderrahmane Kheddar and Olivier Tempier

Abstract—This paper considers dynamic stair climbing with the HRP-4 humanoid robot as part of an Airbus manufacturing use-case demonstrator. Apart from the fact that HRP-4 had never been challenged to this scenario before, we share experimental knowledge gathered in achieving this task. We also show how walking stabilization based on linear inverted pendulum tracking [1] can be extended with quadratic programming-based wrench distribution and a whole-body admittance controller that relies on both end-effector and CoM strategies. While existing stabilizers tend to use either one or the other of these two approaches, experiments suggest that their combination can improve tracking performance. We demonstrate this solution in a hardware experiment where HRP-4 climbs a staircase with 18.5-cm steps, and release our walking controller as open source software.¹

I. INTRODUCTION

Recently, humanoid robotics has reached a maturity that allows considering deployments in large-scale manufacturing (*e.g.* airplane and shipyards assembly), construction sites and nuclear power-plant dismantling applications. These environments are populated with stairs. In the case of airplane manufacturing, stairs allow workers to travel between different shop-floor levels. Hence, among other reasons, it is advantageous to have humanoid automation solution in such applications. As for now however, there is no certification nor performance measurements in terms of requirements and safety to evaluate our algorithms. Although climbing stairs was demonstrated as early as the first release of the Honda humanoid robot in 1997, it is still a challenging task. As a matter of fact, the winner humanoid robot that climbed stairs at the DARPA Robotics Challenge, made it backwards due to the problem of knee-stair contact while walking with bent knees. Robust stabilization is critical during stair climbing, especially in environments where human workers are present.

In order to correct the deviation of their measured state from a reference walking pattern, walking controllers for position-controlled robots need to servo their contact forces with the environment, that is to say, to implement *admittance control*. To the exception of Honda humanoid robots², controllers found in the literature implement this in one of

The authors are with the Montpellier Laboratory of Informatics, Robotics and Microelectronics (LIRMM), CNRS–University of Montpellier, France. A. Kheddar is also with the CNRS–AIST Joint Robotics Laboratory (JRL), UMI3218/RL, Japan. This work is supported in part by the H2020 EU project COMANOID <http://www.comanoid.eu/>, RIA No 645097.

¹https://github.com/stephane-caron/lipm_walking_controller/

²Controllers reported by Honda include the *model ZMP control* strategy [2], [3] where saturation of ZMP constraints triggers recovery CoM accelerations and a corresponding update of the walking pattern [4], [5]. This integration of a switching control law with replanning behavior makes these controllers more advanced than linear feedback controllers.

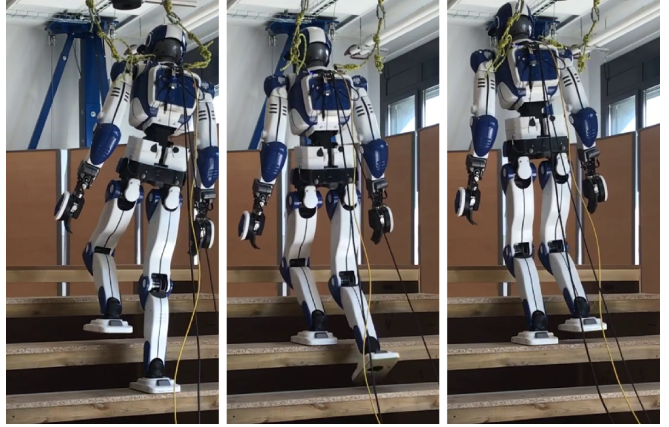


Fig. 1. HRP-4 humanoid climbing a staircase with 18.5-cm steps.

two ways: either by end-effector admittance control [1], [6], [7], [8] or by CoM admittance control [9], [10], [11], [12]. Yet, these two strategies are not mutually exclusive. In the present work, we investigate an implementation of whole-body admittance control where both end-effector and CoM strategies are applied simultaneously. Preliminary analysis in stair climbing simulations and experiments suggests that a combination of these two approaches can improve tracking performance.

Figure 2 illustrates the components implemented in our walking and stair climbing controller. The two main components for stabilization are:

- *Contact Wrench Control* (Section II), which computes contact wrenches to compensate deviations from the walking pattern.
- *Whole-body Admittance Control* (Section III), which realizes the desired contact wrenches on the position-controlled robot.

We illustrate the performance of this controller in a hardware experiment where the HRP-4 humanoid climbs a staircase with 18.5 cm steps. To the best of our knowledge, this is the first time that dynamic stair climbing is demonstrated with HRP-4. The controller used in this experiment is also open source and open to comments.¹

II. CONTACT WRENCH CONTROL

The goal of this first component is to regulate the robot’s first-order dynamics assuming control of its second-order dynamics. This amounts to decide a *net contact wrench* that compensates deviations from the walking pattern.

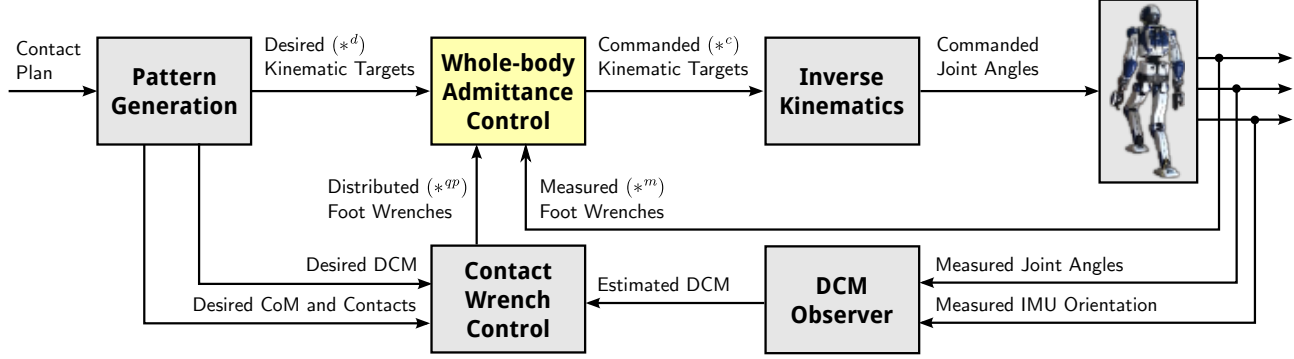


Fig. 2. Overview of the walking controller presented in this manuscript: ...

Within the equations of motion of an articulated robot [13], the centroidal dynamics is governed by the Newton-Euler equation:

$$\begin{bmatrix} m\ddot{\mathbf{c}} \\ \dot{\mathbf{L}}_c \end{bmatrix} = \begin{bmatrix} \mathbf{f} \\ \tau_c \end{bmatrix} + \begin{bmatrix} mg \\ \mathbf{0} \end{bmatrix} \quad (1)$$

where m denotes the total robot mass, \mathbf{g} is the gravity vector, \mathbf{c} the position of the center of mass (CoM) and \mathbf{L}_c the angular momentum around \mathbf{c} . The net contact wrench (\mathbf{f}, τ_c) consists of the resultant \mathbf{f} of the external contact forces applied to the robot and their moment τ_c around the center of mass \mathbf{c} . The left-hand side of this equation corresponds to the net motion of the robot, while the right-hand side represents its interaction with the environment. The gist of locomotion is to leverage these interaction forces to move the CoM (or similarly the translation of the floating base) to a desired location.

A. Linear Inverted Pendulum Mode

A general walking pattern generator [14] can provide both a CoM trajectory $\mathbf{c}(t)$ and an angular-momentum trajectory $\mathbf{L}_c(t)$. Alternatively, the problem can be reduced to providing a single CoM trajectory by considering only solutions where $\mathbf{L}_c(t) = \mathbf{0}$. The resulting model, known as the Inverted Pendulum Mode (IPM) [15], is expressive enough for walking or stair climbing. It simplifies Equation (1) to:

$$\ddot{\mathbf{c}} = \lambda(\mathbf{c} - \mathbf{z}) + \mathbf{g} \quad (2)$$

where the contact wrench is now characterized by a positive scaling factor λ and a *zero-tilting moment point* (ZMP) \mathbf{z} .

Another working assumption suitable for walking over a horizontal surface is to assume a constant CoM height $c_z = h$ above that surface. This gives rise to the Linear Inverted Pendulum Mode (LIPM) [16]:

$$\ddot{\mathbf{c}} = \omega^2(\mathbf{c} - \mathbf{z}) \quad (3)$$

where $\omega = \sqrt{g/h}$, and we drop from now on the gravity vector by considering only horizontal coordinates. The LIPM linearizes the dynamics (2) of the IPM by turning the variable λ into a constant. Its contact wrench is characterized by the position \mathbf{z} of the ZMP on the contact surface.

These simplifications come at the expense of balance recovery strategies: the IPM sacrifices the hip strategy [17]

while the LIPM sacrifices the height-variation strategy [18], [19]. Accordingly, the dimension of the contact wrench decreases from six to three in the IPM and two in the LIPM. A LIPM-based stabilizer such as the one reported in the present paper can leverage these two force coordinates to control two position coordinates, for instance the horizontal position of the center of mass [1] or the rolling and pitching angles of the floating base [3].

B. Feedback of the Divergent Component of Motion

The *divergent component of motion* (DCM) of the LIPM is defined by:

$$\xi = \mathbf{c} + \frac{\dot{\mathbf{c}}}{\omega} \quad (4)$$

It allows a decomposition of the second-order equation (3) into two coupled first-order systems [4]:

$$\dot{\xi} = \omega(\xi - \mathbf{z}) \quad (5)$$

$$\dot{\mathbf{c}} = \omega(\xi - \mathbf{c}) \quad (6)$$

While the DCM naturally diverges away from the ZMP by Equation (5), Equation (6) shows that the CoM is guaranteed to converge to the DCM without being controlled. It is therefore sufficient for locomotion to control only the DCM, rather than *e.g.* the CoM position and velocity.

Walking pattern generation provides a trajectory $\mathbf{c}^d(t)$ satisfying the linear inverted pendulum mode (3), from which one can derive $\xi^d(t)$ and $\mathbf{z}^d(t)$. The DCM can be controlled around this reference by proportional feedback [20], [21]:

$$\dot{\xi} = \dot{\xi}^d + k_p(\xi^d - \xi) \quad (7)$$

where k_p is a positive feedback gain. An integral term can be added to eliminate steady-state error [7], which would correspond here to an offset between the CoM and ZMP positions when the robot is in static equilibrium:

$$\dot{\xi} = \dot{\xi}^d + k_p(\xi^d - \xi) + k_i \int (\xi^d - \xi) \quad (8)$$

The integral term can be complemented by an anti-windup strategy such as saturation.³

³We used a decay factor $\int x = \int_{t=0}^T x(t) \exp(\gamma(t-T))dt$ with $\gamma = 0.2$ Hz, which ensures $\int x \leq (1/\gamma) \|x\|_\infty$ and whose implementation does not require storing a sliding window in memory.

From Equation (5), this control law can be written in terms of the ZMP:

$$\mathbf{z} = \mathbf{z}^d - \left[1 + \frac{k_p}{\omega} \right] (\boldsymbol{\xi}^d - \boldsymbol{\xi}) - \frac{k_i}{\omega} \int (\boldsymbol{\xi}^d - \boldsymbol{\xi}) \quad (9)$$

Or equivalently in terms of the net contact wrench:

$$\begin{bmatrix} \mathbf{f} \\ \boldsymbol{\tau}_c \end{bmatrix} = m \begin{bmatrix} \omega^2(\mathbf{c} - \mathbf{z}) - \mathbf{g} \\ \mathbf{0} \end{bmatrix} \quad (10)$$

DCM feedback is thus a way to determine a net contact wrench that includes both a feedforward term from the walking pattern and a feedback term to correct CoM position and velocity deviations from their reference.

C. Contact Wrench Distribution

While stabilizers based on CoM admittance control [9], [11], [12], [22] take the net wrench as only input, those that include foot force control need to distribute this wrench among contacts. This operation corresponds to the ZMP distribution rules of the stabilizer by Kajita *et al.* [1]. Meanwhile, the net wrench obtained by DCM feedback needs to be saturated in order to account for feasibility constraints such as keeping the ZMP inside its support area. Both distribution and saturation operations can be handled at once by formulating the wrench distribution problem as a *quadratic program* (QP).

We will make use of spatial vector algebra [23] to describe this program. Let us denote by ${}^0\mathbf{w}_{ext}$ the net contact wrench coordinates from Equation (10) expressed in the inertial frame 0 . Define ${}^{lc}\mathbf{w}_{left}$ and ${}^{la}\mathbf{w}_{left}$ the left foot contact wrench expressed respectively in the left sole center frame lc and ankle frame la (closest to the ankle joint). The wrenches ${}^{rc}\mathbf{w}_{right}$ and ${}^{ra}\mathbf{w}_{right}$ are defined similarly.

1) *Constraints*: in double support, the wrench distribution QP consists of two constraints. First, the contact-stability condition:

$$\mathbf{U}^{lc}\mathbf{w}_{left} \leq 0 \quad \mathbf{U}^{rc}\mathbf{w}_{right} \leq 0 \quad (11)$$

where \mathbf{U} is the 16×6 matrix of the *contact wrench cone* [24]. This matrix includes all three components of the contact-stability condition: the resultant-force friction cone, center-of-pressure area and yaw-moment variable boundaries.

Second, a minimum pressure at each contact:

$$e_{fz}{}^{lc}\mathbf{w}_{left} \geq p_{min} \quad e_{fz}{}^{rc}\mathbf{w}_{right} \geq p_{min} \quad (12)$$

where e_{fz} is the basis vector that selects the resultant pressure of a wrench, and we used $p_{min} = 15$ N in practice. This constraint avoids sending low-pressure targets to the foot force controller, as fixed-gain admittance control tends to oscillate around contact switches for such targets.

2) *Costs*: the cost function of the wrench distribution QP weighs three objectives. First and foremost, the solution should realize the net contact wrench as close as possible:

$$\|{}^0\mathbf{w}_{left} + {}^0\mathbf{w}_{right} - {}^0\mathbf{w}_{ext}\|^2 \quad (13)$$

Second, it should minimize ankles torques:

$$\|{}^{la}\mathbf{w}_{left}\|_{\mathbf{W}_{ankle}}^2 + \|{}^{ra}\mathbf{w}_{right}\|_{\mathbf{W}_{ankle}}^2 \quad (14)$$

where \mathbf{W}_{ankle} is a diagonal weight matrix with 1 for ankle torques and a very small value ϵ for all other components. Finally, the pressure ratio should be as close as possible to a prescribed value ρ :

$$\|(1 - \rho)e_{fz}{}^{lc}\mathbf{w}_{left} - \rho e_{fz}{}^{rc}\mathbf{w}_{right}\|^2 \quad (15)$$

This last term is added to regularize the discontinuity in force outputs that occurs in second-order QP formulations [25], [8] when adding or removing contacts. The prescribed pressure ratio ranges from $\rho_{init} \in \{0, 1\}$ at the beginning of the double support phase to $1 - \rho_{init}$ at the end of it.

Although we presented and implemented it as a quadratic program, this optimization is in essence a lexicographic optimization [26] whose four levels are (11)–(12), (13), (14) and (15). We approximate this behavior by setting cost weights to 10000 for (13), 100 for (14) and 1 for (15). Note that the latter two costs are omitted during single support where there is no force redundancy and the net-wrench cost (13) suffices to define a single optimum.

III. WHOLE-BODY ADMITTANCE CONTROL

Whole-body admittance control implements feedback control of the desired force targets issued by contact wrench control, while otherwise following the position targets (CoM, foot and pelvis frames) provided in the walking pattern. In this component, we propose a combination of both the end-effector and centroidal approaches to contact wrench feedback control.

A. Foot damping control

Admittance control applied at the ankle joint has been referred to as ground reaction force control [2], [3], foot damping control [1] or foot adjusting control [11]. It implements the first stabilization strategy from Section 4.5.1 of the *Introduction to Humanoid Robotics* [27].

Let us denote by (θ_r^c, θ_p^c) the *commanded* (see Figure 2) roll and pitch angles of the ankle joint of a foot in contact with the environment. We apply the following damping control law:⁴

$$\frac{d}{dt} \begin{bmatrix} \theta_r \\ \theta_p \end{bmatrix} = \mathbf{A}_{cop}(\mathbf{p}^{qp} \times \mathbf{f}^m - \boldsymbol{\tau}^m) \quad (16)$$

$$\mathbf{A}_{cop} \equiv \begin{bmatrix} A_{cop,y} & 0 & 0 \\ 0 & A_{cop,x} & 0 \end{bmatrix} \quad (17)$$

where $\mathbf{p}^{qp} = [p_x^{qp} \ p_y^{qp} \ 0]$ denotes the target CoP position in the foot frame provided by the wrench distribution QP, and $(\mathbf{f}^m, \boldsymbol{\tau}^m)$ is the measured contact wrench expressed at the origin of the foot frame. The matrix \mathbf{A} of admittance gains $(A_{cop,x}, A_{cop,y})$ is used to tune the responsiveness of the task: a higher $A_{cop,y}$ implies that the foot will roll faster in reaction to lateral CoP deviations, and similarly a higher $A_{cop,x}$ implies that the foot will pitch faster in reaction to sagittal CoP deviations.

Equation (16) is adapted from [1], with the slight difference that we track the desired CoP rather than a desired

⁴Damping control is a shorthand for first-order admittance control.

torque. The two approaches are equivalent under accurate foot pressure difference tracking, but in situations where the latter is degraded, the CoP formulation naturally defines the pressure-dependent admittance coefficients identified in [28]. This task can also be extended to include integral and derivative terms of the measured wrench [8]. Importantly, it can also be improved by a model of the flexibility located between the ankle joint and foot sole [3], [29], which we did not include in the present work.

B. Foot force difference control

In a walking gait, double support phases are used to transfer the “weight” (actually the contact pressure) from one support foot to the next. It is therefore helpful to servo not only the CoP targets provided at each foot, but also their pressure. For this purpose, Kajita *et al.* [1], [30] introduced *foot force difference control* (FFDC). Denoting by (v_{Lz}, v_{Rz}) the respective velocities of the left and right foot in their sole frames, FFDC can be implemented as:

$$v_{Lz}^c = v_{Lz}^d - 0.5v_{\delta fz} + 0.5v_{vdc} \quad (18)$$

$$v_{Rz}^c = v_{Rz}^d + 0.5v_{\delta fz} + 0.5v_{vdc} \quad (19)$$

$$v_{\delta fz} \equiv A_{\delta fz} [(f_{Lz}^{qp} - f_{Rz}^{qp}) - (f_{Lz}^m - f_{Rz}^m)] \quad (20)$$

$$v_{vdc} \equiv T_{vdc}^{-1} [(p_{Lz}^d + p_{Rz}^d) - (p_{Lz}^c + p_{Rz}^c)] \quad (21)$$

The velocity term $v_{\delta fz}$ implements a damping control that lifts the foot in excess of pressure and lowers the other one. The second velocity term v_{vdc} is added for vertical drift compensation. It retrieves the same average foot altitude as in the walking pattern. This choice of a velocity formulation (18)–(21) of FFDC rather than the position one from [1] is contingent to our inverse kinematics and should yield the same behavior.

An implicit side effect of FFDC is that it *increases CoM compliance*. To illustrate this remark, consider the example of a constant external push applied to laterally: with only foot damping control, the robot will resist it by tilting its feet, while with FFDC it will lift the leg opposite to the push, resulting (as gravity maintains contact) in a CoM displacement toward that leg. As such, we may venture to say that our reference controller [1] implicitly included a form of CoM admittance control.

C. CoM Admittance Control

Admittance control applied at the CoM has been referred to as ZMP compliance control [9], ZMP damping control [11], position-based ZMP control [12] or horizontal compliance control [31]. It implements the third stabilization strategy from Section 4.5.1 of the *Introduction to Humanoid Robotics* [27], and should not be confused with the model ZMP control (fifth strategy) applied on Honda robots [2], [3], [5]. The former adds CoM accelerations at all times, the latter only upon saturation of a ZMP constraint.

We apply the following admittance control law:

$$\ddot{\mathbf{c}}^c = \ddot{\mathbf{c}}^d + \mathbf{A}_{com}(\mathbf{z}^m - \mathbf{z}^{qp}) \quad (22)$$

$$\mathbf{A}_{com} \equiv \begin{bmatrix} A_{com,x} & 0 & 0 \\ 0 & A_{com,y} & 0 \end{bmatrix} \quad (23)$$

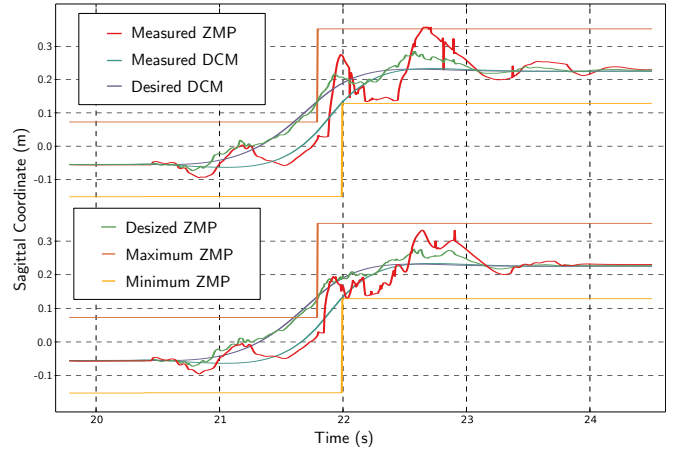


Fig. 3. Effect of applying CoM admittance control in combination with both foot damping control laws. In this simulation, the robot steps on a 18.5-cm step but tilts back on its heel during left-foot support. **Top:** $A_{com,x} = 0$ and $A_{com,y} = 0$. **Bottom:** $A_{com,x} = 20$ and $A_{com,y} = 10$. In both experiments, $A_{cop,x} = A_{cop,y} = 0.005$ and $A_{\delta fz} = 0.0001$.

where $\ddot{\mathbf{c}}^d$ is the feedforward CoM acceleration from the walking pattern, \mathbf{z}^m is the ZMP of the measured net contact wrench and \mathbf{z}^{qp} is the ZMP of the net contact wrench output by the distribution QP (Section II-C). The matrix \mathbf{A}_{com} of admittance gains ($A_{com,x}, A_{com,y}$) is used to tune the responsiveness of the task: the higher the gain, the faster the CoM will accelerate toward the measured ZMP \mathbf{z}^m in order to bring it closer to the target.

Figure 3 shows a simulation example of step climbing without and with CoM admittance control, both foot damping control laws being active. The CoM admittance law does not seem to conflict with the end-effector ones. On the contrary, it improves both DCM and ZMP tracking noticeably.

D. Inverse Kinematics

Commanded velocities and accelerations are sent to a weighted task-based inverse kinematics solver [8], [25]. The following tasks are considered simultaneously:

- Maintain foot contact(s) (weight: 10000)
- CoM position and velocity tracking (weight: 1000)
- Swing foot position and velocity tracking (weight: 500)
- Bend the chest to a prescribed angle (weight: 100)
- Keep the pelvis upright (weight: 10)
- Regularizing half-sitting joint configuration (weight: 10)

Each task implements an acceleration-based tracking law:

$$\ddot{\mathbf{x}} = K(\mathbf{x}^c - \mathbf{x}) + B(\dot{\mathbf{x}}^c - \dot{\mathbf{x}}) + \ddot{\mathbf{x}}^c \quad (24)$$

Task damping coefficients B are set by default to their critical value $2\sqrt{K}$, with the exception of foot contact tasks where we use $B = 300$ Hz and $K = 1$ Hz². In single support where foot force difference control is disabled, the translation stiffness of the support foot task is increased to $K = 1000$ Hz² for vertical drift compensation.

IV. EXPERIMENTS

We implemented the controller described in Figure 2 (see the Appendix for details on other components) and

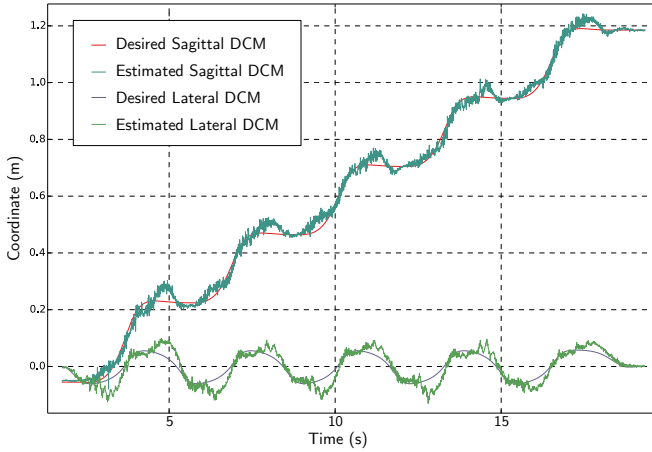


Fig. 4. DCM tracking performance while climbing a staircase with 18.5-cm steps. Swing leg motions are not accounted for in the walking pattern and drive the DCM away from its reference at each step. These disturbances are compensated by the stabilizer in both sagittal and lateral directions.

carried out hardware experiments on the HRP-4 humanoid robot [32].

A. Experimental setup

Our setup consists of lab-made wooden stairs that reproduce the dimensions of the staircase that will be climbed to access the assembly area in the final demonstrator of the COMANOID project (Airbus scale 1 : 1 aircraft). It consists of five steps with length 24 cm and height 18.5 cm.

In order to secure the robot, we used a cable-driven parallel robot developed in our laboratory consisting of eight actuators, from which we used four. Cables were attached to a tailored holding system connecting safety ropes to the shoulders of HRP-4. This system is remote-controlled by a human to track the robot during the climbing experiments. The operator makes sure that the safety ropes stay loose, while trying to avoid hitting the robot.

B. Results

We confirmed that HRP-4 can dynamically climb the target staircase, as shown in Figure 1 and in the accompanying video. In our experiments, DCM gains were set to $k_p = 5$ and $k_i = 1$, while admittance and inverse kinematics gains were respectively:

$A_{cop,x}$	$A_{cop,y}$	$A_{\delta\bar{z}}$	$A_{com,x}$	$A_{com,y}$
0.1	0.1	0.0001	20	10
K_{com}	K_{swing}	K_{chest}	K_{pelvis}	$K_{posture}$
1000	2000	10	10	1

The robot climbs the stairs in 18 s. Its contact plan contains ten steps, and its gait is timed by 1.4 s single-support and 0.2 s double-support durations. DCM and ZMP tracking performance are respectively reported in Figures 4 and 5. To avoid collisions, the apex of swing foot trajectories for each step is set to 24 cm, which is a first source of DCM disturbance. The second main cause are the CoM height variations at each step that disturb the horizontal ZMP.

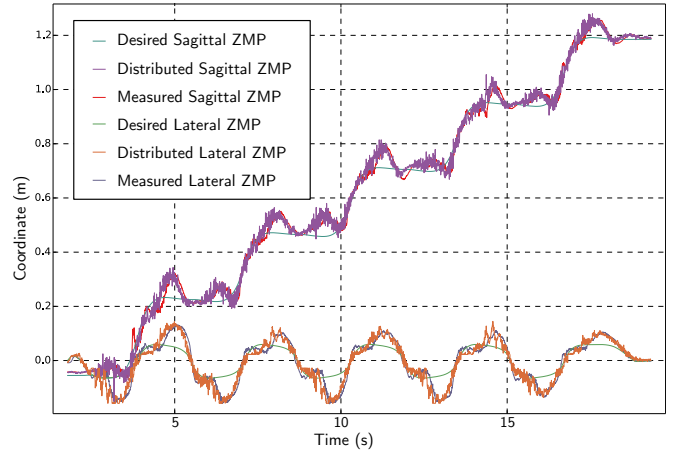


Fig. 5. ZMP tracking performance while climbing a staircase with 18.5-cm steps. During leg swings, the distributed ZMP is driven away from the walking pattern reference to compensate for DCM errors. Whole-body admittance control successfully regulates the ZMP to the distributed one.

backwards. We mitigated this by delaying CoM lift to the end of the step, unfortunately thus increasing knee torques as well. A better way to improve this in future work will be to switch to a pattern generation method taking height variations into account [19], [21], [33].

C. Practicalities

One of the most precious tools at our disposal during our trials and errors was the Chorenoid⁵ dynamics simulator [34], in which we could reproduce most of the phenomena we encountered in practice. The ability to test controllers in fast simulations rather than slow experiments is a serious enabler, and for humanoid robotics, Chorenoid outperforms alternatives like V-REP or Gazebo in terms of both realism and real-time performance.

During our first hardware experiments, the robot would systematically servo-off during the second (and most knee-torque intensive) swing phase of step climbing. This behavior was due to a drop of voltage imposed by a maximum current setting of 5 A on the power supply. We progressively increased this threshold and observed peak current draws reaching up to 13 A. We estimate the peak power consumption to be around 750 W. For comparison, ASIMO consumes 600–900 W when its servomotors are turned on, and around 1000 W during stair climbing [35]. This consumption gap is mostly owed to the lightweight design of HRP-4 [32], which is both lighter (40 kg versus 50 kg) and taller than its Honda sibling (1.5 m versus 1.3 m), allowing it to bend its knees less while climbing.

Our initial plan was to climb (i) a single step, (ii) the staircase with double-support phases over each step, and finally (iii) a more human-like stair climbing with exactly one foot contact per step. We presently report on (ii) but not (iii), as a technical issue with its mechanical transmission prevents our robot, for the time being, from performing with its right leg the motions that it achieves with the left one.

⁵<http://chorenoid.org/en/>

V. RELATED STAIR CLIMBING WORKS

Stair climbing for bipeds with ZMP-based stabilizers started as early as 1993, when the Honda E6 prototype climbed staircases thanks to the introduction of the stabilization methods developed by Takenaka [35]. This method was showcased in 1997 for the public release of the P2 humanoid robot [2]. Stair climbing was also demonstrated in 2002 on the prototype HRP-1S of the HRP series [11].

However, the stabilizer component provided with robots of the HRP series is mainly designed for walking on overall level ground. Climbing over small staircases with 10-cm steps has been reported on HRP-2 [14], [36], walking with bent knees to avoid undesired behavior close to the knee singularity. In [6], KHR-2 climbed stairs with 12-cm steps. In [14], HRP-2 also climbed stairs with 15-cm steps while grabbing a handrail.

Step heights above 20 cm have been demonstrated, yet with slower gaits. In [37], HRP-4 climbed a 24-cm step, but without stabilization and with a quasi-static motion lasting more than 80 s. During the DARPA Robotics Challenge, six teams successfully climbed a staircase with four 23-cm steps, yet using slow motions and doing frequent pauses as a result of the challenge's conditions (*e.g.* teleoperation with limited network and robots operating untethered) [38], [39]. Dynamic stair climbing for step heights in the 15–30 cm range found in industrial environments seems close but is not commonplace yet.

VI. CONCLUSION

In this paper, we reported on the state-of-the-art of walking stabilization based on linear inverted pendulum tracking and suggested two improvements: a wrench distribution quadratic program, inspired by the methods well-known in multi-contact control, and a whole-body admittance controller combining both end-effector and CoM strategies. We applied the resulting controller in a dynamic stair climbing experiment over 18.5-cm steps, corresponding to the setting of an Airbus manufacturing use-case demonstrator.

Our stabilizer has a number of gain parameters to tune, some of which interact with each other. For instance, lowering foot CoP admittances allows one to raise the DCM feedback gain k_p to larger values before reaching the unstable regime. To model this phenomenon, [1], [7] reduced the joint action of all admittance control laws to a first-order ZMP delay, and chose the gains of DCM feedback control by pole placement for this simplified system. Future work will require us to investigate this question, and at least another one: how to prevent or mitigate touchdown impacts?

ACKNOWLEDGMENTS

The authors would like to warmly thank Kévin Chappellet for his help with robot hardware, Daniele De Simone and Arnaud Tanguy for their kind assistance with experiments, and Pierre-Brice Wieber for helpful and friendly discussions. The cable-driven parallel robot used to secure HRP-4 during our experiments was realized thanks to the support of the European Union through FEDER Grant No 49793.

APPENDIX

A. Walking Pattern Generation

We generate walking patterns using the linear model predictive control approach [40] over pre-defined footstep locations. The corresponding QP minimizes a weighted combination of three costs:

- ZMP deviation from a reference (weight: 1000)
- CoM velocity deviation from a reference (weight: 10)
- CoM jerk (weight: 1)

The reference ZMP trajectory $z_{ideal}(t)$ consists of straight lines connecting foot ankles, while the reference CoM velocity is contact-plan specific and set to zero by default. The QP also enforces the following constraints:

- Feasibility: ZMPs lie in their support polygons
- Terminal constraint 1: the ZMP ends on $z_{ideal}(T)$
- Terminal constraint 2: the DCM ends on $z_{ideal}(T)$

where $T = 1.6$ s is the duration of the predictive horizon and the sampling period is set to 100 ms. We let predictive control update the CoM reference $c^d(t)$ and its derivatives by open-loop forward integration rather than a closed-loop approach [41].

B. DCM observer

Estimating the divergent component of motion is an important part for a stabilizer based on DCM tracking control. Although we plan to evaluate methods that take into account foot flexibilities [42], [43], for now we are using the following kinematics estimator. Consider an anchor point p_a^c of the commanded robot model (output of the inverse kinematics) assumed to be in contact with the ground on the real robot. Then, the orientation of the floating-base is read directly from the robot's IMU, and its translation is computed so that $p_a^m = p_a^c$. Once the floating-base has been estimated, the CoM position is derived by forward kinematics on joint-encoder readings, and its velocity is obtained via a first-order low-pass frequency filter with cutoff period $T_{cutoff} = 10$ ms.

Note that choosing fixed anchor points depending on the number of contacts [1] can yield discontinuous estimates at contact switches. To avoid this, we interpolate the anchor point p_a continuously during double support phases based on the index ρ used in Equation (15).

REFERENCES

- [1] S. Kajita, M. Morisawa, K. Miura, S. Nakaoka, K. Harada, K. Kaneko, F. Kanehiro, and K. Yokoi, “Biped walking stabilization based on linear inverted pendulum tracking,” in *IEEE/RSJ International Conference on Intelligent Robots and Systems*, 2010, pp. 4489–4496.
- [2] K. Hirai, M. Hirose, Y. Haikawa, and T. Takenaka, “The development of honda humanoid robot,” in *International Conference on Robotics and Automation*, 1998.
- [3] T. Takenaka, T. Matsumoto, and T. Yoshiike, “Real time motion generation and control for biped robot-4th report: Integrated balance control,” in *IEEE/RSJ International Conference on Intelligent Robots and Systems*, 2009.
- [4] —, “Real time motion generation and control for biped robot-1st report: Walking gait pattern generation,” in *IEEE/RSJ International Conference on Intelligent Robots and Systems*, Oct. 2009.
- [5] T. Kamioka, H. Kaneko, T. Takenaka, and T. Yoshiike, “Simultaneous optimization of ZMP and footsteps based on the analytical solution of divergent component of motion,” in *IEEE International Conference on Robotics and Automation*, May 2018, p. 8.

[6] J.-Y. Kim, I.-W. Park, and J.-H. Oh, "Realization of dynamic stair climbing for biped humanoid robot using force/torque sensors," *Journal of Intelligent and Robotic Systems*, vol. 56, no. 4, 2009.

[7] M. Morisawa, S. Kajita, F. Kanehiro, K. Kaneko, K. Miura, and K. Yokoi, "Balance control based on capture point error compensation for biped walking on uneven terrain," in *IEEE-RAS International Conference on Humanoid Robots*, 2012.

[8] K. Bouyarmane, K. Chappellet, J. Vaillant, and A. Kheddar, "Multi-robot and task-space force control with quadratic programming," *IEEE Transactions on Robotics*, 2019, to appear.

[9] K. Nagasaka, "Whole-body motion generation for a humanoid robot by dynamics filters," *PhD thesis*, 1999, the Univ. of Tokyo, in Japanese.

[10] T. Sugihara and Y. Nakamura, "Whole-body cooperative balancing of humanoid robot using COG jacobian," in *IEEE/RSJ International Conference on Intelligent Robots and Systems*, 2002, p. 6.

[11] K. Yokoi, F. Kanehiro, K. Kaneko, S. Kajita, K. Fujiwara, and H. Hirukawa, "Experimental study of humanoid robot HRP-1s," *The International Journal of Robotics Research*, vol. 23, no. 4, pp. 351–362, Apr. 2004.

[12] J. Englsberger and C. Ott, "Integration of vertical COM motion and angular momentum in an extended capture point tracking controller for bipedal walking," in *IEEE-RAS International Conference on Humanoid Robots*. IEEE, 2012, pp. 183–189.

[13] P.-B. Wieber, "Some comments on the structure of the dynamics of articulated motion," in *Fast motions in biomechanics and robotics*, 2006, pp. 411–425.

[14] J. Carpentier and N. Mansard, "Multi-contact locomotion of legged robots," May 2017, pre-print.

[15] J. E. Pratt and S. V. Drakunov, "Derivation and application of a conserved orbital energy for the inverted pendulum bipedal walking model," in *IEEE International Conference on Robotics and Automation*, May 2007, pp. 4653–4660.

[16] S. Kajita, F. Kanehiro, K. Kaneko, K. Yokoi, and H. Hirukawa, "The 3d linear inverted pendulum mode: A simple modeling for a biped walking pattern generation," in *IEEE/RSJ International Conference on Intelligent Robots and Systems*, vol. 1, Sep. 2001, pp. 239–246.

[17] B. Stephens, "Humanoid push recovery," in *IEEE-RAS International Conference on Humanoid Robots*, Nov. 2007, pp. 589–595.

[18] T. Koolen, M. Posa, and R. Tedrake, "Balance control using center of mass height variation: Limitations imposed by unilateral contact," in *IEEE-RAS International Conference on Humanoid Robots*, Nov. 2016.

[19] S. Caron and B. Mallein, "Balance control using both ZMP and COM height variations: A convex boundedness approach," in *IEEE International Conference on Robotics and Automation*, May 2018, p. 6.

[20] T. Sugihara, "Standing stabilizability and stepping maneuver in planar bipedalism based on the best com-zmp regulator," in *IEEE International Conference on Robotics and Automation*, 2009.

[21] J. Englsberger, C. Ott, and A. Albu-Schäffer, "Three-dimensional bipedal walking control based on divergent component of motion," *IEEE Transactions on Robotics*, vol. 31, no. 2, 2015.

[22] Z. Li, C. Zhou, N. Tsagarakis, and D. Caldwell, "Compliance control for stabilizing the humanoid on the changing slope based on terrain inclination estimation," *Autonomous Robots*, vol. 40, no. 6, pp. 955–971, Aug. 2016.

[23] R. Featherstone, *Rigid body dynamics algorithms*. Springer, 2008.

[24] S. Caron, Q.-C. Pham, and Y. Nakamura, "Stability of surface contacts for humanoid robots: Closed-form formulae of the contact wrench for rectangular support areas," in *IEEE International Conference on Robotics and Automation*, May 2015, pp. 5107–5112.

[25] L. Saab, O. E. Ramos, F. Keith, N. Mansard, P. Soueres, and J.-Y. Fourquet, "Dynamic whole-body motion generation under rigid contacts and other unilateral constraints," *IEEE Transactions on Robotics*, vol. 29, no. 2, pp. 346–362, Apr. 2013.

[26] A. Escande, N. Mansard, and P.-B. Wieber, "Hierarchical quadratic programming: Fast online humanoid-robot motion generation," *The International Journal of Robotics Research*, vol. 33, no. 7, 2014.

[27] S. Kajita, H. Hirukawa, K. Harada, and K. Yokoi, *Introduction to Humanoid Robotics*, ser. Springer Tracts in Advanced Robotics. Springer Berlin Heidelberg, 2014, vol. 101.

[28] A. Pajon, S. Caron, G. De Magistris, S. Miossec, and A. Kheddar, "Walking on Gravel with Soft Soles using Linear Inverted Pendulum Tracking and Reaction Force Distribution," in *IEEE-RAS International Conference on Humanoid Robots*, 2017.

[29] S. Kajita, K. Yokoi, M. Saigo, and K. Tanie, "Balancing a humanoid robot using backdrive concerned torque control and DIrect angular momentum feedback," in *IEEE International Conference on Robotics and Automation*, 2001.

[30] S. Kajita, F. Asano, M. Morisawa, K. Miura, K. Kaneko, F. Kanehiro, and K. Yokoi, "Vertical vibration suppression for a position controlled biped robot," in *IEEE International Conference on Robotics and Automation*, 2013, pp. 1637–1642.

[31] Z. Li, B. Vanderborght, N. G. Tsagarakis, L. Colasanto, and D. G. Caldwell, "Stabilization for the compliant humanoid robot COMAN exploiting intrinsic and controlled compliance," in *IEEE International Conference on Robotics and Automation*, 2012, pp. 2000–2006.

[32] K. Kaneko, F. Kanehiro, M. Morisawa, K. Akachi, G. Miyamori, A. Hayashi, and N. Kanehira, "Humanoid robot HRP-4 - humanoid robotics platform with lightweight and slim body," in *IEEE/RSJ International Conference on Intelligent Robots and Systems*, Sep. 2011, pp. 4400–4407.

[33] C. Brasseur, A. Sherikov, C. Collette, D. Dimitrov, and P.-B. Wieber, "A robust linear MPC approach to online generation of 3d biped walking motion," in *IEEE-RAS International Conference on Humanoid Robots*, 2015, pp. 595–601.

[34] S. Nakaoka, S. Hattori, F. Kanehiro, S. Kajita, and H. Hirukawa, "Iterative contact force solver for simulating articulated rigid bodies," in *RSJ 2007*, 2007, in Japanese.

[35] M. Hirose, "The father of the bipedal walking robot ASIMO," *Takeda Foundation Survey Reports*, Jun. 2007, in Japanese.

[36] P. Michel, J. Chestnutt, Satoshi Kagami, Koichi Nishiwaki, James Kuffner, and Takeo Kanade, "GPU-accelerated real-time 3d tracking for humanoid locomotion and stair climbing," in *IEEE/RSJ International Conference on Intelligent Robots and Systems*, Oct. 2007.

[37] T. Zhang, S. Caron, and Y. Nakamura, "Supervoxel plane segmentation and multi-contact motion generation for humanoid stair climbing," *International Journal of Humanoid Robotics*, vol. 14, Mar. 2017.

[38] J. Lim, I. Lee, I. Shim, H. Jung, H. M. Joe, H. Bae, O. Sim, J. Oh, T. Jung, S. Shin, K. Joo, M. Kim, K. Lee, Y. Bok, D.-G. Choi, B. Cho, S. Kim, J. Heo, I. Kim, J. Lee, I. S. Kwon, and J.-H. Oh, "Robot system of DRC-HUBO+ and control strategy of team KAIST in DARPA robotics challenge finals," *Journal of Field Robotics*, 2016.

[39] M. Johnson, B. Shrewsbury, S. Bertrand, D. Calvert, T. Wu, D. Duran, D. Stephen, N. Mertins, J. Carff, W. Rifenburgh, J. Smith, C. Schmidt-Wetekam, D. Faconti, A. Gruber-Tilton, N. Eyslette, T. Meier, I. Kalkov, T. Craig, N. Payton, S. McCrory, G. Wiedebach, B. Layton, P. Neuhaus, and J. Pratt, "Team IHMCs lessons learned from the DARPA robotics challenge: Finding data in the rubble," in *The DARPA Robotics Challenge Finals: Humanoid Robots To The Rescue*, M. Spenko, S. Buerger, and K. Iagnemma, Eds. Springer International Publishing, 2018, vol. 121, pp. 71–102.

[40] P.-B. Wieber, "Trajectory free linear model predictive control for stable walking in the presence of strong perturbations," in *IEEE-RAS International Conference on Humanoid Robots*, Nov. 2006.

[41] N. A. Villa and P.-B. Wieber, "Model predictive control of biped walking with bounded uncertainties," in *IEEE-RAS International Conference on Humanoid Robots*, Nov. 2017, pp. 836–841.

[42] M. Benallegue, A. Benallegue, and Y. Chitour, "Tilt estimator for 3d non-rigid pendulum based on a tri-axial accelerometer and gyrometer," in *IEEE-RAS International Conference on Humanoid Robots*, Nov. 2017, pp. 830–835.

[43] T. Flayols, A. Del Prete, P. Wensing, A. Mifsud, M. Benallegue, and O. Stasse, "Experimental evaluation of simple estimators for humanoid robots," in *IEEE-RAS International Conference on Humanoid Robots*, Nov. 2017.